ACS APPLIED MATERIALS & INTERFACES

Research Article

www.acsami.org

High-Performance and Stable Gel-State Dye-Sensitized Solar Cells Using Anodic TiO_2 Nanotube Arrays and Polymer-Based Gel Electrolytes

Zahra Seidalilir,[†] Rasoul Malekfar,*[,†] Hui-Ping Wu,[‡] Jia-Wei Shiu,[‡] and Eric Wei-Guang Diau*[,‡]

[†]Atomic and Molecular Group, Physics Department, Tarbiat Modares University, P.O. Box 14115-175, Tehran, Iran

[‡]Department of Applied Chemistry and Institute of Molecular Science, National Chiao Tung University, Hsinchu 30010, Taiwan

Supporting Information

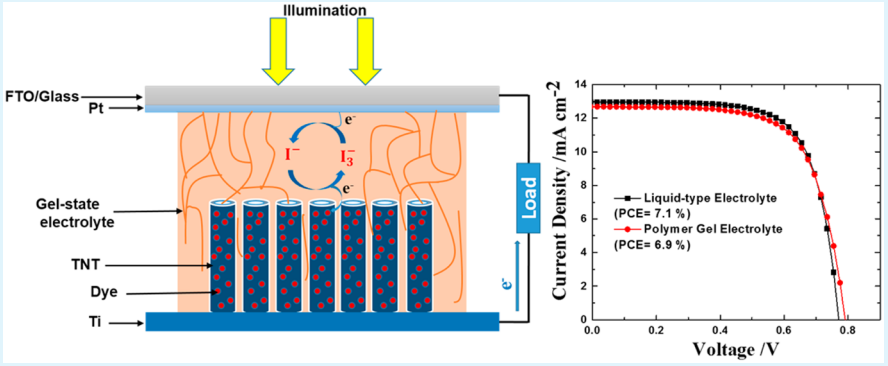

ABSTRACT: Highly ordered and vertically oriented TiO_2 nanotube (NT) arrays were synthesized with potentiostatic anodization of Ti foil and applied to fabricate gel-state dye-sensitized solar cells (DSSCs). The open structure of the TiO_2 NT facilitates the infiltration of the gel-state electrolyte; their one-dimensional structural feature provides effective charge transport. TiO_2 NTs of length L = 15−35 μm were produced on anodization for periods of t = 5−15 h at a constant voltage of 60 V, and sensitized with N719 for photovoltaic characterization. A commercially available copolymer, poly(methyl methacrylate-*co*-ethyl acrylate) (PMMA-EA), served as a gelling agent to prepare a polymer-gel electrolyte (PGE) for DSSC applications. The PGE as prepared exhibited a maximum conductivity of 4.58 mS cm^{-1} with PMMA-EA (7 wt %). The phase transition temperature (T_p) of the PGE containing PMMA-EA at varied concentrations was determined on the basis of the viscosities measured at varied temperatures. T_p increased with increasing concentration of PMMA-EA. An NT-DSSC with L = 30 μm assembled using a PGE containing PMMA-EA (7 wt %) exhibited an overall power conversion efficiency (PCE) of 6.9%, which is comparable with that of a corresponding liquid-type device, PCE = 7.1%. Moreover, the gel-state NT-DSSC exhibited excellent thermal and light-soaking enduring stability: the best device retained ∼90% of its initial efficiency after 1000 h under 1 sun of illumination at 50 °C, whereas its liquid-state counterpart decayed appreciably after light soaking for 500 h.

KEYWORDS: *anodization, DSSC, polymer-gel electrolyte, PMMA-EA, TiO_2 nanotubes*

1. INTRODUCTION

Dye-sensitized solar cells (DSSCs) have attracted intensive attention because of their great device performance and fabrication at a modest cost.[1] In a conventional DSSC, an electron-collecting layer (photoanode) is composed of a three-dimensional network of randomly interconnected TiO_2 nanoparticles (NPs). The photovoltaic efficiency of power conversion (PCE) of an NP-DSSC employing sensitizers based on zinc porphyrin dyes and a cobalt(II/III) tris-(bipyridyl)-based redox electrolyte exceeded 12.3%,[2] but the utilization of liquid electrolytes raises several practical problems, including the leakage of the liquid solvent, possible desorption of the adsorbed photosensitizers, and corrosion of the Pt counter electrode; these factors cause poor enduring stability of the device for practical applications.[3] An approach to avoid these problems is to replace the liquid electrolyte with solid-state or gel-state electrolytes, such as organic or inorganic hole-transport materials,[4,5] ionic liquids,[6] polymer electrolytes,[7] and gel materials incorporating redox couples.[8] In a solid-state DSSC without a liquid solvent, the small ionic conductivity and poor interfacial contact between the solid electrolyte and the TiO_2 photoelectrode produce a poor cell performance.[9] Quasi-solid-state electrolytes, such as polymer-gel electrolytes (PGEs),[3,10] are reported to attain sufficient penetration of the electrolyte into the porous photoelectrode.

Received: February 16, 2015
Accepted: May 18, 2015
Published: May 18, 2015

DOI: 10.1021/acsami.5b01519
ACS Appl. Mater. Interfaces 2015, 7, 12731−12739

A polymer-gel electrolyte is a quasi-solid-state electrolyte of a particular kind that involves a state of electrolyte intermediate between liquid and solid. In a PGE, the polymer host acts as a gelling agent and provides a three-dimensional network in the polymer cages that effectively traps the liquid electrolyte. Free movement of cations and anions in the solution phase trapped by the polymer cages is the major factor responsible for the ionic conductivity of the PGE, but if the applied polymer has the ability to solvate the cations effectively, both solid and liquid phases in the PGE can participate in ionic transport inside the polymer cages.[11] Through their unique hybrid network structure, PGEs thus have the mechanical properties of solids but the diffusive transport characteristics of liquids.[12] PGEs thereby possess several advantages such as small leakage, large ionic conductivity, effective interfacial contact with TiO_2, and enduring stability.[13−16] To date, various polymers and copolymers such as poly(methyl methacrylate) (PMMA),[17] poly(acrylonitrile-*co*-vinyl acetate) (PAN-VA),[18] poly(vinylidene fluoride-*co*-hexafluoropropene) (PVDF-HFP),[19] and poly(methyl methacrylate-*co*-methacrylate acid)/poly(ethanediol) (PMMA-*co*-MAA)/PEG[20] have served as gelators to prepare PGEs for DSSC applications, even though quasi-solid-state electrolytes generally feature a large viscosity. Poor infiltration of PGEs into the mesoporous TiO_2 photoelectrodes consisting of NP layers hence becomes a major problem for quasi-solid-state DSSCs to achieve superior device performance.[21] Trap-limited diffusion for electron transport in randomly packed TiO_2 NPs is another drawback for photoanodes of this kind.[22] TiO_2 nanostructures that facilitate the penetration of viscous PGEs and offer a capability to improve charge transport are essential to enhance the performance of gel-type DSSCs of this kind.

The size difference between the mesopores in the photoanode and the coils of the polymeric chain of the polymers leads to a poor infiltration of the polymer electrolytes. TiO_2 photoanodes with one-dimensional (1D) nanostructures such as nanowires,[22] nanofibers,[23] nanorods,[24] and nanotubes (NTs)[25] are good candidates to improve the pore-filling property of a polymer electrolyte into the TiO_2 nanopores. For example, the gel-state DSSC incorporated with an electrospun-made TiO_2 nanofiber electrode yielded a PCE of 4.6%.[23] The pore size of the TiO_2 film is an important issue for gel-state DSSCs, for which Kim and co-workers reported that the device performance of a quasi-solid-state DSSC based on the organized mesoporous TiO_2 nanostructure is 2 times greater than those of the devices made of randomly packed TiO_2 films.[26] Nogueira and co-workers applied randomly packed TiO_2 NT films as a photoanode for a solid-state DSSC and found that the device performance with the NT film is greater than that with the nanoparticles.[25] Therefore, the use of spatially oriented 1D TiO_2 nanostructures as photoanodes for DSSCs is expected to significantly improve the efficiency of charge collection by promoting rapid electron transport and slow charge recombination, in particular for the anodic growth of vertically oriented 1D TiO_2 NT arrays from a titanium foil. Anodic TiO_2 NT arrays are superior to nanowires or nanorods because of their increased surface area for dye adsorption at longer tube lengths.[27] Many researchers have thus focused on using TiO_2 NT arrays as a prospective photoanode in both liquid-type DSSCs[28−33] and solid-state DSSCs.[25,34,35] However, there has appeared no report of TiO_2 NT arrays used as a photoanode in a gel-type DSSC based on polymer-gel electrolytes.

In the present work, we utilized a copolymer—poly(methyl methacrylate-*co*-ethyl acrylate) (PMMA-EA)—to solidify a liquid electrolyte based on acetonitrile (ACN) to form a PGE of a new type. We investigated the mechanism of diffusion and conduction of the PMMA-EA gel electrolyte and compared it with that of an ACN-based liquid electrolyte. Figure 1 shows

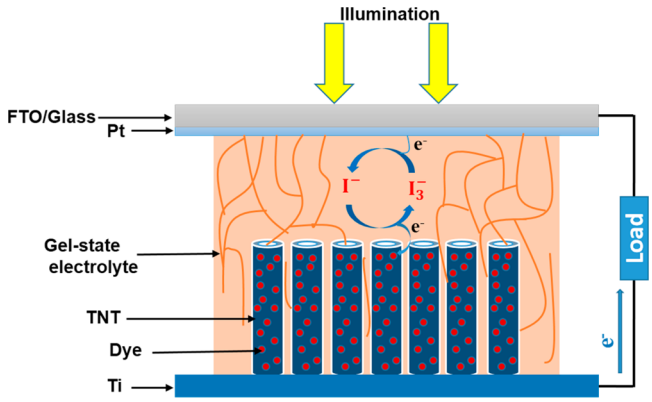

Figure 1. Schematic representation of the device configuration and working mechanism for a gel-state NT-DSSC under rear illumination.

the configuration of the device and the working principle for a TiO_2 NT-based gel-state DSSC. The use of a TiO_2 NT film as a photoanode prospectively solves the major drawback of the pore-filling problem in gel-state DSSCs. We used anodization to synthesize TiO_2 NT arrays with nanotubes of length L = 15−35 μm. The best performance of the NT-DSSC devices using an ACN-based liquid redox electrolyte was obtained with a PCE of 7.1% at $L \approx 30$ μm. With the new polymer-gel electrolyte containing PMMA-EA (7 wt %), we constructed an NT-DSSC with a tube length of ~30 μm exhibiting an impressive PCE of 6.9% under 1 sun of irradiation and remarkable enduring stability under thermal and light-soaking conditions.

2. EXPERIMENTS

2.1. Synthesis of Anodic TiO_2 NT Arrays. Highly ordered TiO_2 NT arrays were fabricated with potentiostatic anodization in an electrochemical cell with two electrodes.[32,33] Ti foil (commercially pure grade 1, purity 99.9%, substrate size 6 × 6 cm^2, thickness 130 μm, Kobe Steel) served as the anode on which TiO_2 NTs grew; another Ti foil of the same size served as the cathode. The two electrodes at a fixed interval of 2.7 cm were placed in a thermostatic container (T = 22 °C) containing the electrolyte solution. The ordered TiO_2 NT arrays were produced in electrolyte solutions containing NH_4F (purity 99.9%, 0.4 wt %) in ethanediol in the presence of H_2O (2 vol %) at 60 V for varied periods. After the anodization, the anodic sample was washed in ethanol and annealed at 450 °C for 1 h to crystallize amorphous TiO_2 into its anatase phase.[27,29−32] To remove a dense layer of unwanted deposit on top of the TiO_2 NT arrays that was introduced during anodization, we ultrasonicated the annealed sample in ethanol for 15 min. We investigated the morphology of the TiO_2 NT films with scanning electron microscopy (SEM; JSM-6390LV, JEOL).

2.2. Post-Treatment of $TiCl_4$. To increase the effective surface area of the tubes and to improve the cell performance, we treated the TiO_2 NT films with $TiCl_4$ in two steps, as reported elsewhere.[32] First, the TiO_2 NT films as prepared were immersed in a $TiCl_4$ solution (0.073 M) at 50 °C for 30 min followed by rinsing with deionized water and drying in an oven at 50 °C. These films were then immersed in a $TiCl_4$ stock solution for 2 h again and sintered at 350 °C for 30 min.

DOI: 10.1021/acsami.5b01519
ACS Appl. Mater. Interfaces 2015, 7, 12731−12739

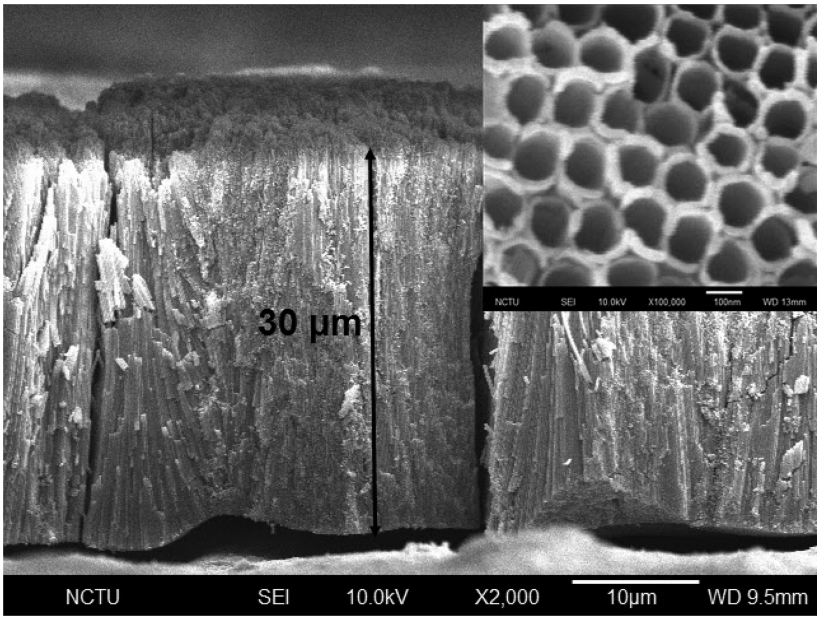

Figure 2. Side-view SEM image of TiO_2 NT arrays with a tube length (L) of 30 μm. The inset shows the corresponding top-view SEM image of the TiO_2 NT arrays.

2.3. Preparation of Electrolytes. The liquid electrolyte consisted of lithium iodide (LiI; 0.1 M), diiodine (I_2; 0.01 M), 4-*tert*-butylpyridine (TBP; 0.5 M), 1-butyl-3-methylimidazolium iodide (BMII; 0.6 M), and guanidinium thiocyanate (GuNCS; 0.1 M) in ACN. To prepare the PGE, we mixed the copolymer PMMA-EA (Aldrich, mean molar mass 101000 g mol^{-1}, ethyl acrylate concentration <5 wt %) with the liquid electrolyte and then heated the mixture with stirring to 70 °C until a viscous solution was obtained. The polymer electrolytes were at first in a sol state, making possible filling of the electrolytes into the cells. A gel-state electrolyte approached over a period of a few days with the temperature maintained near 23 °C. Cooling is reported to significantly increase the rate of gelation of the electrolytes.[18] The duration of gelation depended on the concentration of the copolymer in the solution; at about −4 °C, the gel-state approached after about 22 h when PMMA-EA (4 wt %) was introduced into the electrolyte. The period of gelation was decreased to about 15, 9, and 3 h for electrolytes containing PMMA-EA (7, 10, and 13 wt %, respectively). The temperature of phase transfer and flow Gibbs energy of the electrolytes were determined on the basis of the viscosities of the electrolytes measured at varied temperatures using a programmable rheometer (DV-III, Brookfield).

2.4. Fabrication of an NT-DSSC. The dye uptake into the anodic TiO_2 NT films (0.4 × 0.4 cm^2) was performed in a solution of N719 dye (3 × 10^{-4} M, Solaronix) containing chenodeoxycholic acid (CDCA; 3 × 10^{-4} M) in acetonitrile/*tert*-butyl alcohol (v/v = 1/1) binary solvent for 18 h. The films were then washed with ethanol to remove the nonchemisorbed dye and dried with gaseous N_2. To fabricate an NT-DSSC device, we combined the N719/TiO_2 NT film as the anode with a transparent Pt counter electrode as the cathode. The counter electrode was made on spin-coating a H_2PtCl_6/2-propanol solution onto a fluorine-doped tin oxide (FTO; 7 Ω sq^{-1})/glass (TEC 7, Hartford Tec Glass Co. Inc., Hartford City, IN) substrate (typical size 1.0 × 1.5 cm^2) through thermal decomposition at 380 °C for 30 min. The NT-DSSC device was sealed with a molten film (SX1170, Solaronix, thickness 60 μm). To inject the electrolytes, we drilled two holes on the counter electrode away from the active area. To prepare a gel-state NT-DSSC, we introduced hot polymer electrolytes as a thin layer into the space between the two electrodes; the holes were then sealed with a spacer and a thin cover glass. The cells were further sealed in two nested polyethylene bags (Ziploc) and kept at about −4 °C to convert the liquid-state polymer electrolyte to a gel-state polymer electrolyte. Silver gel was coated on the counter electrode to decrease the series resistance of the device.

2.5. Examination of Dye Loading. To measure the amount of N719 dye absorbed on the anodic TiO_2 NT films, we desorbed the dye in a basic solution (tetrabutylammonium hydroxide ((TBA)OH), 0.1 M in methanol).[36] The absorption spectrum of the solution was recorded with a UV−vis spectrometer (Varian, Cary50). A calibration curve for dye N719 in (TBA)OH (0.1 M) in methanol was derived to obtain the absorption coefficient, 13610 M^{-1} cm^{-1} at 516 nm. The amount of dye adsorbed on the TiO_2 NT films, summarized in Table S1, Supporting Information, was obtained from the measured absorbance (cuvette thickness 3 mm) at 516 nm and the absorption coefficient obtained from the calibration curve according to a linear relation.

2.6. Characterization of Photovoltaic Impedance. The current−voltage characteristics were measured with a digital source meter (Keithley 2400, computer controlled) with the device under 1 sun of illumination (AM-1.5G, 100 mW cm^{-2}) from a solar simulator (XES-40S1, SAN-EI) calibrated with a standard silicon reference cell (VLSI Standards, Oriel PN 91150 V). The spectra of the efficiency of conversion of incident photons to current (IPCE) of the corresponding devices were recorded with a system consisting of a Xe lamp (PTiA-1010, 150 W), a monochromator (PTi, 1200 gr mm^{-1} blazed at 500 nm), and a source meter (Keithley 2400). The photovoltaic performance of an NT-DSSC was characterized with illumination from the back side; the transparent counter electrode was covered with a black plastic mask of the same size as the anode, 0.16 cm^2, for all measurements. The ionic conductivity and diffusion coefficient of the electrolytes were calculated from the EIS (electrochemical impedance spectroscopy) spectra measured with an electrochemical system (IM6, Zahner). We measured the impedance of the electrolytes with a symmetric cell configuration, Pt/electrolyte/Pt. The frequency range was 0.01 Hz to 1 MHz; the magnitude of the alternating potential was 20 mV. To analyze the EIS data, we fitted them to an equivalent circuit with simulation software (Z-view).

3. RESULTS AND DISCUSSION

3.1. Effect of the Tube Length on the Photovoltaic Performance of NT-DSSCs. To optimize the tube length of the TiO_2 NT arrays as photoanodes for gel-state DSSCs, we undertook anodization of Ti foil in the electrolyte solution at a constant voltage of 60 V for periods of 5, 9, 12, and 15 h, which

DOI: 10.1021/acsami.5b01519
ACS Appl. Mater. Interfaces 2015, 7, 12731−12739

produced TiO_2 NT films with tube lengths of 15, 22, 30, and 35 μm, respectively. The corresponding SEM side-view images are shown in Figure S1, Supporting Information. Figure 2 shows an SEM image of the TiO_2 NT arrays with a tube length of 30 μm; the inset shows that the average pore diameter on top of the TiO_2 NT films is ~100 nm. These TiO_2 NT films post-treated with $TiCl_4$ were sensitized with N719 dye and used to fabricate liquid-state NT-DSSC devices; the corresponding current–voltage characteristics and IPCE action spectra appear in parts a and b, respectively, of Figure S2, Supporting Information. The corresponding photovoltaic parameters are presented in Table S1, Supporting Information. Measurements of dye loading (Figure S3, Supporting Information) provided the amount of adsorbed dye molecules on the $TiCl_4$-post-treated TiO_2 NT films (Table S1), which confirmed that longer tubes possess a larger surface area for dye adsorption. We observed that the quality of the TiO_2 NT films at L = 35 μm was less than for the shorter tubes, and the adhesion to the substrate of the long tubes was poorer than for the shorter tubes. The cell performance thus increased from η = 5.9% at L = 15 μm to η = 7.0% at L = 30 μm but decreased slightly to η = 6.6% at L = 35 μm (Table S1). According to the photovoltaic results summarized in Table S1, L = 30 μm is the optimum length of tube to attain the maximum efficiency of power conversion, consistent with our previous results.[30,32] TiO_2 NT arrays with L = 30 μm thus served as photoanodes in the fabrication of gel-state NT-DSSCs.

3.2. Effects of the Concentration of PMMA-EA on the Properties of the Electrolytes. Polymer-gel electrolytes (PMMA-EA, 4–13 wt % in acetonitrile) were prepared. To test the effect of the concentration of PMMA-EA on the performance of the polymer-gel electrolytes, we measured the ionic conductivity, diffusion coefficient, and charge-transfer resistance at the Pt/electrolyte interface (R_{pt}) in a symmetric cell. Figure 3 shows Nyquist plots obtained for the electrolytes containing copolymer PMMA-EA in varied amounts; the semicircles at small frequency (right) correspond to the Nernst diffusion of charge in the electrolytes, whereas those at large frequency (left) correspond to the charge transfer at the Pt/electrolyte interface.[37]

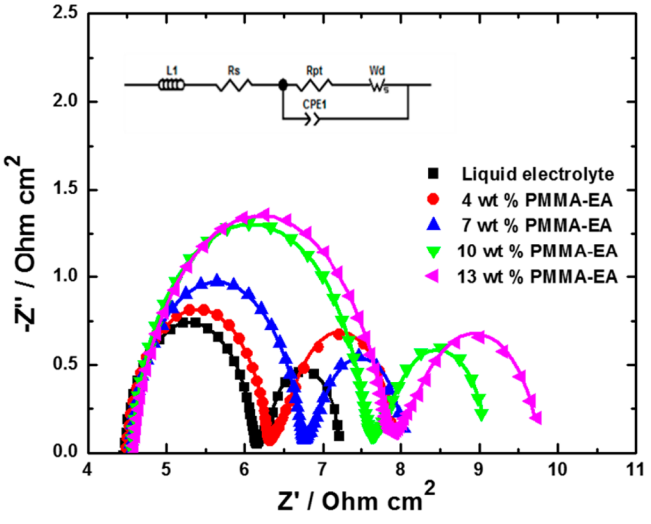

Figure 3. Nyquist plots of EIS spectra measured for electrolytes prepared using PMMA-EA copolymer at varied concentrations. Symbols illustrate the measured data, and solid curves represent the fitted results obtained from simulations based on the equivalent circuit model shown in the inset.

The electrical conductivity of the electrolytes was calculated with the equation $\sigma = l/R_bA$ with the thickness (l) of the PGE, bulk resistance (R_b) determined from the complex impedance plot, and delimited area (A) of the Pt electrode. We measured the conductivities of the electrolytes containing PMMA-EA in varied amounts near 23 °C; the results are summarized in Table 1. As a reference, the conductivity of the polymer-free ACN-based liquid electrolyte was determined to be 5.51 mS cm^{-1}. The value of σ decreased to 3.75 mS cm^{-1} on addition of PMMA-EA (4 wt %) to the PGE, but with increasing concentration of PMMA-EA, the conductivity increased to 4.58 mS cm^{-1} at 7 wt % but decreased on further increase.

Because the amount of iodide much exceeded that of triiodide in the electrolyte, we assumed that the concentration of I^- anions remained constant; only a small contribution of I^- is attributed to the diffusion impedance.[38] Nernst diffusion impedance (Z_N) thus describes the diffusion of I_3^- in the electrolyte. The measured diffusion coefficients of I_3^- with a diffusion-limited current and with Nernst impedance methods were reported to agree satisfactorily.[39] The Nernst impedance is expressible in the following form:[39]

$$Z_N = R_D \frac{1}{\sqrt{\frac{i\omega}{D_1/\delta^2}}} \tanh \sqrt{\frac{i\omega}{D_1/\delta^2}} \quad (1)$$

$$R_D = \frac{K_B T}{m^2 q^2 N_A C^* D_1 \delta} \quad (2)$$

$$D_1 = \frac{1}{2.5}\delta^2 \omega_{max} \quad (3)$$

in which appear the temperature (T), Avogadro constant (N_A), concentration of I_3^- in the bulk (C^*), number of electrons transferred in each reaction (m), diffusion coefficient of I_3^- (D_1), thickness of the electrolyte film (δ), and maximum frequency of the semicircles at small frequency (ω_{max}). As Table 1 shows, the diffusion coefficient of triiodide in the electrolytes systematically decreased with increasing concentration of copolymer. The diffusivity of I_3^- was 7.21 × 10^{-6} cm^2 s^{-1} in the liquid electrolyte, and decreased to 2.96 × 10^{-6} cm^2 s^{-1} in the PGE containing PMMA-EA (13 wt %).

The trend of the concentration of PMMA-EA with ion conductivity differed from that of the diffusivity of I_3^- in the same PGE system. According to early results,[40,41] the characteristic of charge transport in an electrolyte does not depend only on ionic diffusivity. Lee and co-workers found that, in a PGE containing copolymer PAN-VA, increasing the concentration of copolymer decreased the diffusion coefficient of I_3^-, but the ionic conductivity decreased at first and then increased with further increased concentration of PAN-VA.[40] The charge-exchange reaction $I^- + I_3^- \rightarrow I_3^- + I^-$, i.e., charge transfer of the Grotthus type, was proposed to account for the mechanism of charge transport in an I^-/I_3^- redox electrolyte.[41] Herein, because of poor interaction of the polymer chains, the ionic conductivity decreased when PMMA-EA (4 wt %) was added to the liquid electrolyte, but for the PGE with PMMA-EA (7 wt %), the copolymer chains efficiently interacted to form a three-dimensional continuous network that enhanced charge transport for the proposed charge-exchange reaction to occur. PMMA is reported not only to act as an inert matrix surrounding the liquid in PMMA-based gel electrolytes but also

DOI: 10.1021/acsami.5b01519
ACS Appl. Mater. Interfaces 2015, 7, 12731–12739

Table 1. Ion Conductivity (σ), Ion Diffusivity (D_1), Charge-Transfer Resistance at the Pt/Electrolyte Interface (R_{pt}), Flow Gibbs Energies (ΔG_l^* and ΔG_g^*), and Temperature of the Phase Transition of Electrolytes Containing PMMA-EA Copolymer at Varied Concentrations

[PMMA-EA], wt %	σ, mS cm^{-1}	D_1, 10^{-6} cm^2 s^{-1}	R_{pt}, Ω cm^2	ΔG_l^*, kJ mol^{-1}	ΔG_g^*, kJ mol^{-1}	temp, K, of phase transition
0	5.51	7.21	1.7			
4	3.75	5.87	1.8	6.9	9.1	321
7	4.58	4.75	2.2	10.0	17.2	326
10	3.95	3.87	3.0	12.6	25.1	330
13	3.05	2.96	3.2	15.0	34.6	333

to interact with the ions and liquid components.[42] PMMA has the ability to solvate cations, which is beneficial for the dissociation of LiI and BMII, leading to increased concentrations of I^- and I_3^-. Such dense and oriented I^-/I_3^- paths thus improve the charge transport based on the exchange reaction. When the concentration of PMMA-EA further increased, the polymer cages interconnected, however, and readily formed aggregates in the electrolyte, leading to a decreased ionic transport. Figure 3 shows that the charge-transfer resistance at the Pt/electrolyte interface (R_{pt}) increased with increasing concentration of PMMA-EA. R_{pt} was 1.7 Ω cm^2 in the liquid electrolyte and increased to 3.2 Ω cm^2 in the PGE containing PMMA-EA (13 wt %). According to the literature, the charge-transfer resistance at the Pt surface is inversely proportional to the roughness factor of the counter electrode.[43] Herein, the adsorption of PMMA-EA copolymer onto the Pt counter might hinder direct contact of the PGE with the counter electrode, and thereby inhibit the reduction of triiodide at the counter electrode, which leads to an increased R_{pt}.

Figure 4a presents the viscosity data of the electrolytes containing PMMA-EA in varied proportions and measured at

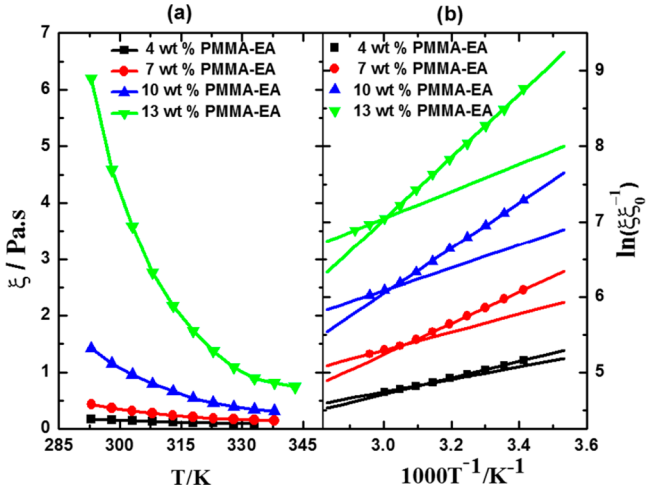

Figure 4. (a) Viscosity (ξ) as a function of temperature (T) and (b) $\ln(\xi\xi_0^{-1})$ vs T^{-1} for electrolytes containing varied concentrations of PMMA-EA copolymer.

varied temperatures. The ACN-based liquid electrolyte exhibited a viscosity of less than 0.001 Pa s near 23 °C. The results show that the viscosity of the electrolytes containing PMMA-EA at varied concentrations decreased exponentially with increasing temperature. These data are correlated with a simplified McAllister equation:[44]

$$\ln(\xi/\xi_0) = \ln(B) + \frac{\Delta G^*}{RT} \quad (4)$$

in which ξ and ξ_0 are the viscosities of the electrolytes in the presence and absence of the copolymer, respectively, ΔG^* denotes the flow Gibbs energy, T the temperature, and R the molar gas constant, and B is a constant over a small temperature range. The physical meaning of ΔG^* is the energy barrier impeding flow in a polymer electrolyte. As shown in Figure 4b for the plots of $\ln(\xi/\xi_0)$ vs T^{-1}, each electrolyte system possessed two values of Gibbs energy corresponding to two distinct phase states of the electrolytes, for which ΔG_g^* and ΔG_l^* represent the flow Gibbs energies in the gel state (lower temperature region) and the liquid state (higher temperature region), respectively. With increasing temperature, the phase state of the PGE transformed from the gel state with a greater viscosity and Gibbs energy to the liquid state with a smaller viscosity and Gibbs energy. Table 1 presents the flow Gibbs energies calculated from the McAllister plot in both the gel (ΔG_g^*) and viscous liquid (ΔG_l^*) states. The results exhibit a systematic trend of ΔG_g^*, in which the Gibbs energy in the gel state increased from ΔG_g^* = 9.1 kJ mol^{-1} at PMMA-EA (4 wt %) to ΔG_g^* = 34.6 kJ mol^{-1} at PMMA-EA (13 wt %). Table 1 lists the temperatures (T_p) of the transition between the gel and liquid phases obtained from the data in Figure 4b. These temperatures systematically increased from T_p = 321 K for the PGE containing PMMA-EA (4 wt %) to T_p = 333 K for the PGE with PMMA-EA (13 wt %).

3.3. Photovoltaic Performance of NT-DSSCs Based on Electrolytes Containing PMMA-EA at Varied Concentrations. Parts a and b of Figure 5 show the $J-V$ characteristics and the corresponding IPCE action spectra of NT-DSSC devices with L = 30 μm and electrolytes containing PMMA-EA at varied concentrations, respectively; Table 2 summarizes the resulting photovoltaic parameters. Because incident light was absorbed by the I^-/I_3^- electrolyte and light was scattered at the Pt-FTO counter electrode, the IPCE values of an NT-DSSC device with rear illumination were less than those of its counterpart front illumination.[30] When PMMA-EA (4 wt %) was added to the liquid electrolyte, J_{SC} of the device decreased. On further addition of the copolymer, J_{SC} increased to attain a maximum at 7 wt %, and then decreased with further increased concentration, consistent with the variation of the ionic conductivity shown in Table 1. V_{OC} of the NT-DSSC increased upon addition of PMMA-EA to 7 wt %, and decreased on further addition of the copolymer. The increased V_{OC} in the PGE-based NT-DSSC compared to its liquid-type counterpart is consistent with the results previously reported.[15,45] The physical phenomenon is explained with the following equation:

$$V_{OC} = \left(\frac{kT}{e}\right)\ln\left(\frac{I_{inj}}{n_{cb}k_{et}[I_3^-]}\right) \quad (5)$$

which involves the Boltzmann constant (k), temperature (T), proton charge (e), incident photon flux (I_{inj}), concentration of

DOI: 10.1021/acsami.5b01519
ACS Appl. Mater. Interfaces 2015, 7, 12731−12739

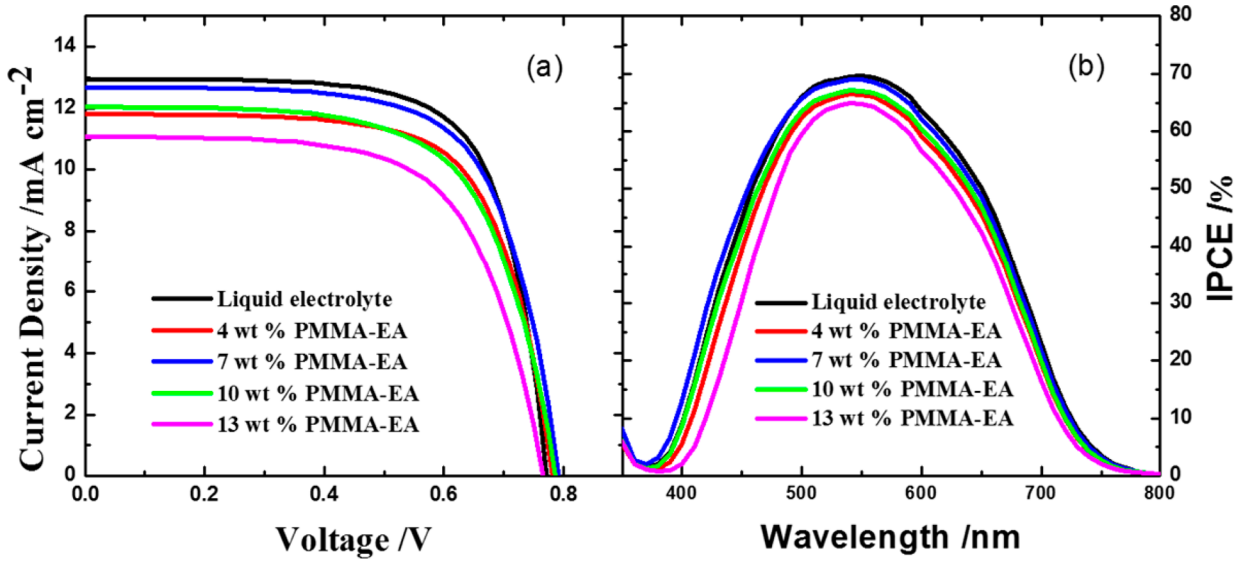

Figure 5. (a) Current−voltage characteristics and (b) IPCE action spectra of NT-DSSC devices with L = 30 μm fabricated with electrolytes containing PMMA-EA copolymer at varied concentrations.

Table 2. Photovoltaic Parameters of NT-DSSC Devices with L = 30 μm Fabricated with Electrolytes Containing PMMA-EA Copolymer at Varied Concentrations under Simulated AM-1.5 Illumination (Power 100 mW cm^{-2}) and an Active Area of 0.16 cm^2

[PMMA-EA], wt %	J_{SC}, mA cm^{-2}	V_{OC}, mV	FF	η, %
0	12.95	771	0.707	7.1
4	11.82	782	0.687	6.4
7	12.68	791	0.684	6.9
10	12.05	786	0.655	6.2
13	11.08	766	0.649	5.5

electrons at the TiO_2 surface (n_{cb}), and coefficient for the rate of charge recombination (k_{et}). V_{OC} of a DSSC was kinetically limited by the charge recombination, whereby the electrons from the conduction band of TiO_2 recombined with I_3^- in the electrolyte. The increased V_{OC} is attributed to the additional function of the PMMA-EA matrix in passivating the active TiO_2 surface and partly suppressing the charge recombination.[15,45] With the copolymer at a larger concentration, the ionic transport decreased as a result of aggregation in the electrolyte (Table 1). The decreased ionic conductivity at larger concentration of PMMA-EA might result in retardation of dye regeneration; then the injected conduction band electrons could have a chance to transfer back into the oxidized dye molecules, leading to a decreased V_{OC}.

Our results show a systematic trend for the fill factor (FF) decreasing with increasing concentration of PMMA-EA. We expect that (1) the increased resistance of charge transfer at the Pt/electrolyte interface due to the adsorption of polymer onto the Pt counter electrode and (2) the decreased penetration of electrolyte inside the TiO_2 nanotubes as a result of the large viscosity of the PGE are responsible for the decreased FF at a greater concentration of PGE. The overall performance of the devices indicates that the best performance of a gel-state NT-DSSC was obtained with PMMA-EA at 7 wt %. The device performance decreased with further increased concentration of the copolymer. For the liquid-state NT-DSSC as a reference, the values are J_{SC} = 12.95 mA cm^{-2}, V_{OC} = 771 mV, FF = 0.707, and η = 7.1%. For the NT-DSSC based on the PGE containing PMMA-EA (7 wt %), the corresponding values of these photovoltaic parameters are respectively 12.68 mA cm^{-2}, 791 mV, 0.684, and 6.9%; the overall efficiency of power conversion of the gel-state NT-DSSC device is comparable with that of its liquid-state counterpart.

There is an intrinsic discrepancy between the present study using anodic TiO_2 NT arrays and many other conventional studies using low-dimensional nanomaterials:[23−26] the TiO_2 NT arrays are vertically oriented on Ti foil, while the conventional 1D TiO_2 nanomaterials are randomly packed in a mesoporous environment on a TCO glass substrate. Our approach thus provides a direct transport channel for ionic conduction when a polymer-gel electrolyte is applied. Although other screen-printing methods can be easily applied to make 1D TiO_2 layers on TCO for front-side illumination,[46] calcination at a high temperature is required. This limits the conventional gel-state DSSC to make a flexible device. In contrast, the anodic TiO_2 NT arrays do not have this problem so that flexible devices can be feasibly fabricated.[29] Moreover, the charge-collection efficiency was much enhanced for the anodic TiO_2 NT films compared to the conventional NP films, as reported by Zhu et al.[47] On the other hand, it has been reported that the efficiencies of the DSSCs based on randomly packed 1D nanostructures were lower than those of traditional DSSCs based on mesoporous nanoparticles due to the problem of insufficient amounts of dye loading for the former case.[46] However, for gel-state electrolytes, these 1D TiO_2 nanostructures may have the potential to improve the device performance of the DSSC due to their excellent pore-filling property and great charge-transport characteristic in comparison with their NP-based counterparts. As pointed out by Kang and co-workers,[48] the increase in the pore size of the photoanode using a variety of TiO_2 nanostructures leads to an improvement in the pore-filling of a polymer electrolyte into the TiO_2 mesopores. According to our approach, the pore diameter of the anodic TiO_2 NT arrays is large enough to facilitate the penetration of the PGE into the TiO_2 NT film. Furthermore, the vertically oriented 1D TiO_2 NT arrays can be produced at a longer tube length to create a larger surface area for sufficient dye adsorption, and the open structure of the nanotubes offers

DOI: 10.1021/acsami.5b01519
ACS Appl. Mater. Interfaces 2015, 7, 12731−12739

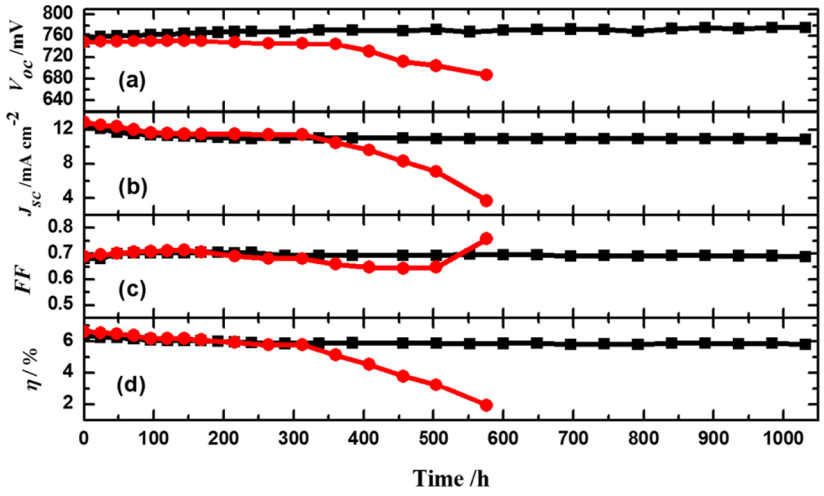

Figure 6. Evaluation of durability over 1000 h for NT-DSSC devices based on a liquid electrolyte (red solid circles) and a PGE containing PMMA-EA (7 wt %, black solid squares) under 1 sun of illumination at 50 °C: (a) V_{OC}; (b) J_{SC}; (c) FF; (d) η.

a great pore-filling property to attain a device performance for the gel-state NT-DSSC comparable to that of the liquid-state counterpart.

3.4. Enduring Stability of NT-DSSCs Based on Liquid and Gel Electrolytes. The stabilities of NT-DSSC devices fabricated with an ACN-based liquid electrolyte and a PGE containing PMMA-EA (7 wt %) in ACN were tested for varied periods under 1 sun of illumination at 50 °C. Because the temperature for the transition from the gel to liquid phase for the PGE containing PMMA-EA (7 wt %) was above 50 °C (Table 1), the PGE inhibited the evaporation of the solvent below 50 °C. Figure 6 shows the variation of the photovoltaic parameters of the two devices as a function of the period over 1000 h under light soaking with 1 sun of irradiation and thermal stress at 50 °C. In the first 200 h, the performance of the gel-state NT-DSSC decreased slightly from η = 6.4% to η = 6.0% and thereafter remained steady. The variation of J_{SC} exhibited a similar trend, but V_{OC} and FF first increased and then remained nearly constant. After light soaking for more than 1000 h, the gel-state NT-DSSC retained 90% of its initial performance. For the liquid-state NT-DSSC, the efficiency of the device decreased slightly from η = 6.6% to η = 6.2% in the first 100 h, and remained nearly constant up to ∼300 h, but the device performance then began to deteriorate; the device efficiency retained less than 30% of its initial value after 570 h. These results indicate that the decreased efficiency of the liquid device was due mainly to the decreased J_{SC}, which is attributed to evaporation of the volatile solvent. Our results thus confirm that the polymer cages in the PGE can efficiently trap the solvent, which can restrain the leakage and evaporation of a liquid electrolyte, therefore leading to a great enduring stability of the device, as we have observed.

4. CONCLUSION

The poor infiltration and trap-limited diffusion for electron transport are two major drawbacks of employing conventional electrodes based on nanoporous TiO_2 NPs in applications in gel-state DSSCs. In this work, we utilized potentiostatic anodization to prepare highly ordered and vertically oriented TiO_2 NT arrays as a photoanode to fabricate gel-state DSSCs. The TiO_2 NTs facilitated the penetration of the gel electrolyte through their open structure, and also improved the transport of charge as a result of their one-dimensional structural nature. The TiO_2 NT films of tube length L = 30 μm were sensitized with N719 dye and fabricated into gel-state devices containing PMMA-EA copolymer in ACN solvent and varied proportions (4, 7, 10, and 13 wt %). The ionic conductivity and diffusivity of the corresponding PGEs in devices with a symmetrical configuration were determined from the measured EIS spectra. The electric conductivity of the PGE was optimum with PMMA-EA at 7 wt %. On the basis of the viscosities measured at varied temperatures, the temperatures (T_p) of the phase transition of these PGEs were determined; T_p exhibited an increasing trend with increasing concentration of PMMA-EA. With the PGE containing PMMA-EA (7 wt %), the NT-DSSC yielded a power conversion efficiency of 6.9%, which is comparable with that of the corresponding liquid electrolyte cell. The gel-state NT-DSSC with PMMA-EA (7 wt %) retained 90% of its initial efficiency over 1000 h under 1 sun of illumination at 50 °C. Because of the superior enduring stability of the device, PMMA-EA is a promising gelator in combination with a TiO_2 NT photoanode for future DSSC applications.

■ ASSOCIATED CONTENT

Supporting Information

Side-view SEM images of the TiO_2 NT arrays with varied tube lengths (Figure S1), J–V characteristics and IPCE action spectra of NT-DSSC devices to find the optimum tube length (Figure S2), UV–vis absorption spectra of the dye-loading experiments (Figure S3), and amount of dye loading and corresponding photovoltaic parameters of NT-DSSC devices as a function of the tube length (Table S1). The Supporting Information is available free of charge on the ACS Publications website at DOI: 10.1021/acsami.5b01519.

■ AUTHOR INFORMATION

Corresponding Authors

*E-mail: malekfar@modares.ac.ir.
*E-mail: diau@mail.nctu.edu.tw.

Notes

The authors declare no competing financial interest.

■ ACKNOWLEDGMENTS

We thank Dr. Hsiu-Ping Jen and Mr. Chien-Hung Shen for their assistance in this work at the initial stage. The Ministry of

DOI: 10.1021/acsami.5b01519
ACS Appl. Mater. Interfaces 2015, 7, 12731–12739

Science and Technology (MOST) of Taiwan supported this work under programs with Contract Numbers NSC 102-2113-M-009-020-MY3, NSC 102-2622-M-009-001-CC1, and NSC 103-2623-E-009-001-ET. Z.S. thanks the National Chiao Tung University (NCTU; Hsinchu, Taiwan) and Iranian Ministry of Science and Technology (Tehran, Iran) for support of her visit to NCTU.

REFERENCES

(1) Hagfeldt, A.; Boschloo, G.; Sun, L.; Kloo, L.; Pettersson, H. Dye-Sensitized Solar Cells. *Chem. Rev.* **2010**, *110*, 6595−6663.
(2) Yella, A.; Lee, H.-W.; Tsao, H. N.; Yi, C.; Chandiran, A. K.; Nazeeruddin, M. K.; Diau, E. W.-G.; Yeh, C.-Y.; Zakeeruddin, S. M.; Grätzel, M. Porphyrin-Sensitized Solar Cells with Cobalt (II/III)-Based Redox Electrolyte Exceed 12% Efficiency. *Science* **2011**, *334*, 629−634.
(3) Wang, P.; Zakeeruddin, S. M.; Moser, J. E.; Nazeeruddin, M. K.; Sekiguchi, T.; Grätzel, M. A Stable Quasi-Solid-State Dye-Sensitized Solar Cell with an Amphiphilic Ruthenium Sensitizer and Polymer Gel Electrolyte. *Nat. Mater.* **2003**, *2*, 402−407.
(4) Wang, M.; Bai, J.; Formal, F. L.; Moon, S.-J.; Cevey-Ha, L.; Humphry-Baker, R.; Grätzel, C.; Zakeeruddin, S. M.; Grätzel, M. Solid-State Dye-Sensitized Solar Cells Using Ordered TiO_2 Nanorods on Transparent Conductive Oxide as Photoanodes. *J. Phys. Chem. C* **2012**, *116*, 3266−3273.
(5) Chung, I.; Lee, B.; He, J.; Chang, R. P. H.; Kanatzidis, M. G. All-Solid-State Dye-Sensitized Solar Cells with High Efficiency. *Nature* **2012**, *485*, 486−489.
(6) Cao, Y.; Zhang, J.; Bai, Y.; Li, R.; Zakeeruddin, S. M.; Grätzel, M.; Wang, P. Dye-Sensitized Solar Cells with Solvent-Free Ionic Liquid Electrolytes. *J. Phys. Chem. C* **2008**, *112*, 13775−13781.
(7) Kim, J. H.; Kang, M.-S.; Kim, Y. J.; Won, J.; Park, N.-G.; Kang, Y. S. Dye-Sensitized Nanocrystalline Solar Cells Based on Composite Polymer Electrolytes Containing Fumed Silica Nanoparticles. *Chem. Commun.* **2004**, 1662−1663.
(8) Wang, Y. Recent Research Progress on Polymer Electrolytes for Dye-Sensitized Solar Cells. *Sol. Energy Mater. Sol. Cells* **2009**, *93*, 1167−1175.
(9) Wang, H.; Li, H.; Xue, B.; Wang, Z.; Meng, Q.; Chen, L. Solid-State Composite Electrolyte LiI/3-Hydroxypropionitrile/SiO_2 for Dye-Sensitized Solar Cells. *J. Am. Chem. Soc.* **2005**, *127*, 6394−6401.
(10) Wang, P.; Zakeeruddin, S. M.; Exnar, I.; Grätzel, M. High Efficiency Dye-Sensitized Nanocrystalline Solar Cells Based on Ionic Liquid Polymer Gel Electrolyte. *Chem. Commun.* **2002**, 2972−2973.
(11) de Freitas, J. N.; Nogueira, A. F.; De Paoli, M.-A. New Insights into Dye-Sensitized Solar Cells with Polymer Electrolytes. *J. Mater. Chem.* **2009**, *19*, 5279−5294.
(12) Nogueira, A. F.; Longo, C.; De Paoli, M.-A. Polymers in Dye Sensitized Solar Cells: Overview and Perspectives. *Coord. Chem. Rev.* **2004**, *248*, 1455−1468.
(13) Wang, L.; Zhang, H.; Wang, C.; Ma, T. Highly Stable Gel-State Dye-Sensitized Solar Cells Based on High Soluble Polyvinyl Acetate. *ACS Sustainable Chem. Eng.* **2013**, *1*, 205−208.
(14) Bella, F.; Ozzello, E. D.; Sacco, A.; Bianco, S.; Bongiovanni, R. Polymer Electrolytes for Dye-Sensitized Solar Cells Prepared by Photopolymerization of PEG-Based Oligomers. *Int. J. Hydrogen Energy* **2014**, *39*, 3036−3045.
(15) Mohan, V. M.; Murakami, K.; Kono, A.; Shimomura, M. Poly(acrylonitrile)/Activated Carbon Composite Polymer Gel Electrolyte for High Efficiency Dye Sensitized Solar Cells. *J. Mater. Chem. A* **2013**, *1*, 7399−7407.
(16) Li, Q.; Chen, X.; Tang, Q.; Cai, H.; Qin, Y.; He, B.; Li, M.; Jin, S.; Liu, Z. Enhanced Photovoltaic Performances of Quasi-Solid-State Dye-Sensitized Solar Cells Using a Novel Conducting Gel Electrolyte. *J. Power Sources* **2014**, *248*, 923−930.
(17) Yang, H.; Huang, M.; Wu, J.; Lan, Z.; Hao, S.; Lin, J. The Polymer Gel Electrolyte Based on Poly(methyl methacrylate) and Its Application in Quasi-Solid-State Dye-Sensitized Solar Cells. *Mater. Chem. Phys.* **2008**, *110*, 38−42.
(18) Chen, C.-L.; Teng, H.; Lee, Y.-L. In Situ Gelation of Electrolytes for Highly Efficient Gel-State Dye-Sensitized Solar Cells. *Adv. Mater.* **2011**, *23*, 4199−4204.
(19) Xiang, W.; Huang, W.; Bach, U.; Spiccia, L. Stable High Efficiency Dye-Sensitized Solar Cells Based on a Cobalt Polymer Gel Electrolyte. *Chem. Commun.* **2013**, *49*, 8997−8999.
(20) Li, P. J.; Wu, J. H.; Huang, M. L.; Hao, S. C.; Lan, Z.; Li, Q.; Kang, S. The Application of P(MMA-*co*-MAA)/PEG Polyblend Gel Electrolyte in Quasi-Solid State Dye-Sensitized Solar Cell at Higher Temperature. *Electrochim. Acta* **2007**, *53*, 903−908.
(21) Hwang, D.; Jo, S. M.; Kim, D. Y.; Armel, V.; MacFarlane, D. R.; Jang, S.-Y. High-Efficiency, Solid-State, Dye-Sensitized Solar Cells Using Hierarchically Structured TiO_2 Nanofibers. *ACS Appl. Mater. Interfaces* **2011**, *3*, 1521−1527.
(22) Law, M.; Greene, L. E.; Johnson, J. C.; Saykally, R.; Yang, P. Nanowire Dye-Sensitized Solar Cells. *Nat. Mater.* **2005**, *4*, 455−459.
(23) Song, M. Y.; Kim, D. K.; Ihn, K. J.; Jo, S. M.; Kim, D. Y. Electrospun TiO_2 Electrodes for Dye-Sensitized Solar Cells. *Nanotechnology* **2004**, *15*, 1861−1865.
(24) Song, M. Y.; Ahn, Y. R.; Jo, S. M.; Kim, D. Y.; Ahn, J.-P. TiO_2 Single-Crystalline Nanorod Electrode for Quasi-Solid-State Dye-Sensitized Solar Cells. *Appl. Phys. Lett.* **2005**, *87*, 113113.
(25) Flores, I. C.; de Freitas, J. N.; Longo, C.; De Paoli, M.-A.; Winnischofer, H.; Nogueira, A. F. Dye-Sensitized Solar Cells Based on TiO_2 Nanotubes and a Solid-State Electrolyte. *J. Photochem. Photobiol., A* **2007**, *189*, 153−160.
(26) Ahn, S. H.; Koh, J. H.; Seo, J. A.; Kim, J. H. Structure Control of Organized Mesoporous TiO_2 Films Templated by Graft Copolymers for Dye-Sensitized Solar Cells. *Chem. Commun.* **2010**, *46*, 1935−1937.
(27) Roy, P.; Kim, D.; Lee, K.; Spiecker, E.; Schmuki, P. TiO_2 Nanotubes and Their Application in Dye-Sensitized Solar Cells. *Nanoscale* **2010**, *2*, 45−59.
(28) Vomiero, A.; Galstyan, V.; Braga, A.; Concina, I.; Brisotto, M.; Bontempi, E.; Sberveglieri, G. Flexible Dye Sensitized Solar Cells Using TiO_2 Nanotubes. *Energy Environ. Sci.* **2011**, *4*, 3408−3413.
(29) Jen, H.-P.; Lin, M.-H.; Li, L.-L.; Wu, H.-P.; Huang, W.-K.; Cheng, P.-J.; Diau, E. W.-G. High-Performance Large-Scale Flexible Dye Sensitized Solar Cells Based on Anodic TiO_2 Nanotube Arrays. *ACS Appl. Mater. Interfaces* **2013**, *5*, 10098−10104.
(30) Li, L.-L.; Tsai, C.-Y.; Wu, H.-P.; Chen, C.-C.; Diau, E. W.-G. Fabrication of Long TiO_2 Nanotube Arrays in a Short Time Using a Hybrid Anodic Method for Highly Efficient Dye-Sensitized Solar Cells. *J. Mater. Chem.* **2010**, *20*, 2753−2758.
(31) Li, L.-L.; Chen, Y.-J.; Wu, H.-P.; Wang, N. S.; Diau, E. W.-G. Detachment and Transfer of Ordered TiO_2 Nanotube Arrays for Front-Illuminated Dye-Sensitized Solar Cells. *Energy Environ. Sci.* **2011**, *4*, 3420−3425.
(32) Chen, C.-C.; Chung, H.-W.; Chen, C.-H.; Lu, H.-P.; Lan, C.-M.; Chen, S.-F.; Luo, L.; Hung, C.-S.; Diau, E. W.-G. Fabrication and Characterization of Anodic Titanium Oxide Nanotube Arrays of Controlled Length for Highly Efficient Dye-Sensitized Solar Cells. *J. Phys. Chem. C* **2008**, *112*, 19151−19157.
(33) Shankar, K.; Mor, G. K.; Prakasam, H. E.; Yoriya, S.; Paulose, M.; Varghese, O. K.; Grimes, C. A. Highly-Ordered TiO_2 Nanotube Arrays up to 220 μm in Length: Use in Water Photoelectrolysis and Dye-Sensitized Solar Cells. *Nanotechnology* **2007**, *18*, 065707.
(34) Stergiopoulos, T.; Ghicov, A.; Likodimos, V.; Tsoukleris, D. S.; Kunze, J.; Schmuki, P.; Falaras, P. Dye-Sensitized Solar Cells Based on Thick Highly Ordered TiO_2 Nanotubes Produced by Controlled Anodic Oxidation in Non-Aqueous Electrolytic Media. *Nanotechnology* **2008**, *19*, 235602.
(35) Chen, P.; Brillet, J.; Bala, H.; Wang, P.; Zakeeruddin, S. M.; Grätzel, M. Solid-State Dye-Sensitized Solar Cells Using TiO_2 Nanotube Arrays on FTO Glass. *J. Mater. Chem.* **2009**, *19*, 5325−5328.
(36) Wu, H.-P.; Ou, Z.-W.; Pan, T.-Y.; Lan, C.-M.; Huang, W.-K.; Lee, H.-W.; Reddy, N. M.; Chen, C.-T.; Chao, W.-S.; Yeh, C.-Y.; Diau,

DOI: 10.1021/acsami.5b01519
ACS Appl. Mater. Interfaces 2015, 7, 12731−12739

E. W.-G. Molecular Engineering of Cocktail Co-Sensitization for Efficient Panchromatic Porphyrin-Sensitized Solar Cells. *Energy Environ. Sci.* **2012**, *5*, 9843−9848.
(37) Tsai, C.-H.; Lu, C.-Y.; Chen, M.-C.; Huang, T.-W.; Wu, C.-C.; Chung, Y.-W. Efficient Gel-State Dye-Sensitized Solar Cells Adopting Polymer Gel Electrolyte Based on Poly(methyl methacrylate). *Org. Electron.* **2013**, *14*, 3131−3137.
(38) Wang, Q.; Moser, J.-E.; Grätzel, M. Electrochemical Impedance Spectroscopic Analysis of Dye-Sensitized Solar Cells. *J. Phys. Chem. B* **2005**, *109*, 14945−14953.
(39) Adachi, M.; Sakamoto, M.; Jiu, J.; Ogata, Y.; Isoda, S. Determination of Parameters of Electron Transport in Dye-Sensitized Solar Cells Using Electrochemical Impedance Spectroscopy. *J. Phys. Chem. B* **2006**, *110*, 13872−13880.
(40) Chen, C.-L.; Teng, H.; Lee, Y.-L. Preparation of Highly Efficient Gel-State Dye-Sensitized Solar Cells Using Polymer Gel Eectrolytes Based on Poly(acrylonitrile-*co*-vinyl acetate). *J. Mater. Chem.* **2011**, *21*, 628−632.
(41) Hoshikawa, T.; Ikebe, T.; Kikuchi, R.; Eguchi, K. Effects of Electrolyte in Dye-Sensitized Solar Cells and Evaluation by Impedance Spectroscopy. *Electrochim. Acta* **2006**, *51*, 5286−5294.
(42) Kim, C. S.; Oh, S. M. Importance of Donor Number in Determining Solvating Ability of Polymers and Tansport Properties in Gel-Type Polymer Electrolytes. *Electrochim. Acta* **2000**, *45*, 2101−2109.
(43) Lee, Y.-L.; Shen, Y.-J.; Yang, Y.-M. A Hybrid PVDF-HFP/Nanoparticle Gel Electrolyte for Dye-Sensitized Solar Cell Applications. *Nanotechnology* **2008**, *19*, 455201.
(44) Wu, J.; Hao, S.; Lan, Z.; Lin, J.; Huang, M.; Huang, Y.; Fang, L.; Yin, S.; Sato, T. A Thermoplastic Gel Electrolyte for Stable Quasi-Solid-State Dye-Sensitized Solar Cells. *Adv. Funct. Mater.* **2007**, *17*, 2645−2652.
(45) Lee, K. S.; Jun, Y.; Park, J. H. Controlled Dissolution of Polystyrene Nanobeads: Transition from Liquid Electrolyte to Gel Electrolyte. *Nano Lett.* **2012**, *12*, 2233−2237.
(46) Wu, H.-P.; Lan, C.-M.; Hu, J.-Y.; Huang, W.-K.; Shiu, J.-W.; Lan, Z.-J.; Tsai, C.-M.; Su, C.-H. Hybrid Titania Photoanodes with a Nanostructured Multi-Layer Configuration for Highly Efficient Dye-Sensitized Solar Cells. *J. Phys. Chem. Lett.* **2013**, *4*, 1570−1577.
(47) Zhu, K.; Neale, N. R.; Miedaner, A.; Frank, A. J. Enhanced Charge-Collection Efficiencies and Light Scattering in Dye-Sensitized Solar Cells Using Oriented TiO_2 Nanotube Arrays. *Nano Lett.* **2007**, *7*, 69−74.
(48) Song, D.; Cho, W.; Lee, J. H.; Kang, Y. S. Toward Higher Energy Conversion Efficiency for Solid Polymer Electrolyte Dye-Sensitized Solar Cells: Ionic Conductivity and TiO_2 Pore-Filling. *J. Phys. Chem. Lett.* **2014**, *5*, 1249−1258.

DOI: 10.1021/acsami.5b01519
ACS Appl. Mater. Interfaces 2015, 7, 12731−12739